Structure, Vol. 12, 2137–2147, December, 2004, ©2004 Elsevier Ltd. All rights reserved. DOI 10.1016/j.str.2004.10.005

Conversion between Three Conformational States of Integrin I Domains with a C-Terminal Pull Spring Studied with Molecular Dynamics

Moonsoo Jin,[1] Ioan Andricioaei,[2,3] and Timothy A. Springer[1,*]
[1]The CBR Institute for Biomedical Research
Department of Pathology
Harvard Medical School
200 Longwood Avenue
Boston, Massachusetts 02115
[2]Department of Chemistry and Biological Chemistry
Harvard University
Cambridge, Massachusetts 02138

Summary

We test with molecular dynamics the hypothesis that interdomain forces in integrins, simulated with a spring attached to the C-terminal α7-helix of an integrin I domain, can allosterically stabilize alternative I domain conformations. Depending on the force applied and timecourse, in α_L and α_M I domains the β6-α7 loop moves successively between three ratchet positions; i.e. from closed to intermediate, and then to open. More distal, linked alterations in MIDAS loops and metal coordination closely resemble those seen when the MIDAS becomes ligated. Simulations show that the intermediate state is populated over a wider range of forces for α_L than α_M I domains. Simulations with mutant I domains suggest that specific ratchet residues regulate conformational equilibria. Simulations with α_1 and α_2 I domains reveal a lack of the intermediate conformation, owing to Phe to Glu substitution at the second ratchet residue. The findings have important implications for biological regulation of integrin adhesiveness.

Introduction

Integrins are a family of noncovalently associated heterodimers of α and β subunits that mediate cell-cell and cell-extracellular matrix interactions (Shimaoka et al., 2002). Each subunit is composed of an extracellular, a transmembrane, and a cytoplasmic domain. Half of the integrin α subunits contain a domain of about 180–190 residues, known as the inserted (I) domain (Figures 1A and 2A). In those integrins, the α I domain is the major ligand binding site (Shimaoka et al., 2002). The α I domain has the dinucleotide binding or Rossman fold, with seven α helices surrounding a central, six-stranded β sheet (Figure 2A). At the top face of the I domain is a metal ion-dependent adhesion site (MIDAS). The β1-α1, α3-α4, and β4-α5 loops contain residues that coordinate the Mg^{2+} ion (Figure 2A) and form the ligand binding site, i.e., the MIDAS (Figure 1B). The distal bottom face of the I domain bears the C- and N-terminal linkers to the β propeller domain (Figure 2A).

*Correspondence: springeroffice@cbr.med.harvard.edu
[3]Present address: Department of Chemistry and the Bioinformatics Program, University of Michigan, Ann Arbor, Michigan 48109.

Integrin $\alpha_L\beta_2$ becomes activated by intracellular signals after other receptors on leukocytes engage ligands. By binding to the intercellular adhesion molecule-1 (ICAM-1) on other cells, $\alpha_L\beta_2$ enables firm adhesion of circulating leukocytes to endothelium, migration within tissues, and cellular immune responses (Springer, 1994). Integrin activation is accompanied by a switchblade-like extension from a bent to an extended conformation (Figures 1A and 1B). This global conformational change is linked to a change in the angle between the β subunit I-like and hybrid domains (Takagi et al., 2002, 2003; Xiao, 2004), activation of a distinct MIDAS in the β I-like domain, and its interaction with a Glu residue in the linker following the α7 helix of the α I domain (Huth et al., 2000; Alonso et al., 2002; Yang et al., 2004) (Figures 1C and 1D). It has been proposed that binding of the Glu to the β I-like domain MIDAS exerts a pull on the α7 helix of the α I domain that allosterically induces conformational change in the ligand binding site at the α I domain MIDAS (Figure 1D) (Lu et al., 2001).

The integrin α_L, α_M, and α_2 I domains have been crystallized in two conformations termed closed and open, and the α_1 I domain has been crystallized in the closed conformation (Lee et al., 1995a, 1995b; Qu and Leahy, 1995, 1996; Kallen et al., 1999; Legge et al., 2000; Shimaoka et al., 2003). Recently, a third, intermediate conformation was revealed for the α_L I domain (Shimaoka et al., 2003). Compared to the low-affinity, closed conformation of the α_L I domain, the intermediate and open conformations have 500- and 10,000-fold higher affinity for ICAM-1, respectively (Shimaoka et al., 2003). Thus far, the intermediate and open conformations of the α_L I domain have only been found for proteins in which these conformations are stabilized by mutationally introduced disulfide bonds connecting the α7 helix to the neighboring β6 strand or α1 helix.

A ratchet consisting of the β6-α7 loop and an underlying hydrophobic pocket stabilizes the α_L I domain in three different conformations (Shimaoka et al., 2003). Residues Leu-295, Phe-292, and Leu-289 in the β6-α7 loop occupy the pocket successively in the closed, intermediate, and open conformations, respectively (Figures 2C and 2D). The upper portion of the α7 helix is a 3_{10} helix, and thus, the occupation of the same pocket by residues three positions apart in sequence (Figure 2F) corresponds to axial, downward displacements of 0, 1, or 2 turns of 3_{10} helix (Figure 2C). Despite the introduced disulfide bond to the α7 helix in the mutant α_L I domain structures, the β6-α7 loop in the open α_L I domain has the same conformation as in wild-type open α_M and α_2 structures (Shimaoka et al., 2003). Furthermore, the β6-α7 loop in the intermediate α_L I domain structure was well packed, with typical B factors; one crystal form diffracted X-rays to 1.3 Å. The well-structured nature of this intermediate conformational state of I domains suggests that it could be present in wild-type $\alpha_L\beta_2$ integrin heterodimers, as well as in other wild-type integrins. If so, it would provide a mechanism for fine regulation of the strength of adhesion (Shimaoka et al., 2003).

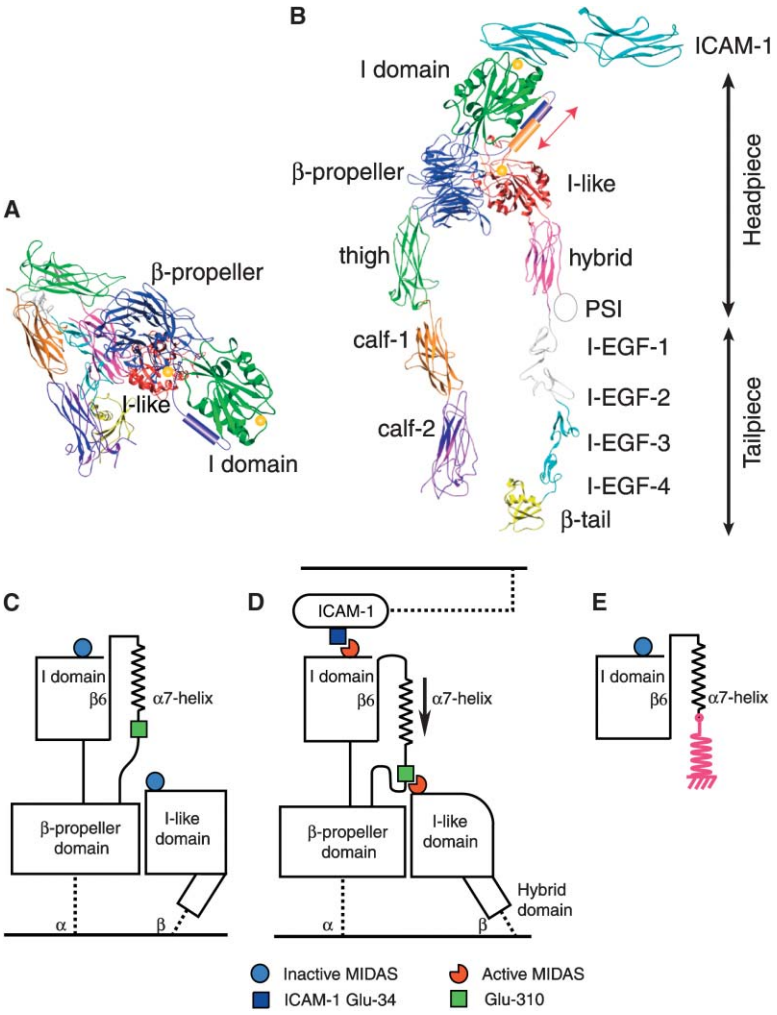

Figure 1. Conformational Change in Integrins with I Domains

(A and B) Ribbon diagrams based on $\alpha_V\beta_3$ crystal and EM structures (Takagi et al., 2002; Xiong et al., 2001) with the I domain or I domain-ICAM-1 complex (Shimaoka et al., 2003) added. (A) Bent conformation of the $\alpha_L\beta_2$ integrin extracellular domain with the closed headpiece and low-affinity I domain. (B) Extended conformation with the open headpiece, high-affinity I domain, and bound ICAM-1. A cylinder symbolizes the position of the α7 helix in the closed (purple) and open (gold) conformations.

(C–E) Schematic diagrams of α7 helix displacement. (C) Low-affinity, closed conformation as in (A). (D) High-affinity, open conformation as in (B). The α7 helix has been pulled down by interaction of α_L-Glu-310 with the β_2 I-like domain MIDAS (Yang et al., 2004). The active MIDAS of the α_L I domain can bind to Glu-34 of ICAM-1 and mediate cell adhesion. (E) The spring (red) attached to the C terminus of the α I domain to mimic, with molecular dynamics, the physiologic activation pathway.

Here, using molecular dynamics simulations with applied external forces (Karplus and McCammon, 2002; Isralewitz et al., 2001) we test a number of hypotheses concerning conformational changes in integrin I domains. The downward, C-terminal pull on the α I domain α7 helix that appears to be exerted in intact integrin heterodimers by an intersubunit interaction (Figure 1D) is simulated with an attached spring of variable strength (Figures 1E and 2E). We examine whether different values of the applied force stabilize the intermediate and open conformations, and whether the intermediate conformation is on the pathway to the open conformation. Simulations with the α_L, α_M, α_1, and α_2 I domains test the hypothesis that substitution of a charged Glu residue for a hydrophobic Phe residue at the intermediate ratchet position in α_1 and α_2 I domains destabilizes the intermediate conformation. The results demonstrate that pulling down on the α7 helix induces the intermediate and open conformations of the β6-α7 loop, and the open conformation at the MIDAS, despite the lack of any explicit favoring of the conformations of these regions in the molecular dynamics simulations. The conformations obtained agree with those seen in crystal structures and support the biological relevance of the intermediate β6-α7 loop conformation trapped in a mutant α_L I domain. The results also suggest that the intermediate I domain conformation can be extended to α_M, but not α_1 and α_2 I domains. Simulations on mutant I domains suggest that variation among I domains in ratchet residues is important in determining the relative stability of the three different I domain conformational states.

Results

Simulation Design and Evaluation

In an intact $\alpha_L\beta_2$ heterodimer, C-terminal axial displacement of the α I domain α7 helix appears to be induced by binding of the linker region following the α7 helix to the β I-like domain in the neighboring β subunit (Figures 1B and 1D). This physiological pulling force on the α7 helix was mimicked by an imaginary harmonic spring (Figures 1D and 1E). The spring was attached to the Cα atom of the C-terminal residue in the α I domain α7 helix, Val-308, and stretched 15 Å by attaching the other end to a fixed point 15 Å along the projection of the helix axis (Figure 2E). The spring constant κ was varied from 0 to 100 pN/Å in approximately 10 pN/Å increments, with ten simulations at each increment. The initial force applied to the C-terminal α helix, $F = \kappa\Delta x$ (where κ is the spring constant and Δx is the spring extension), thus

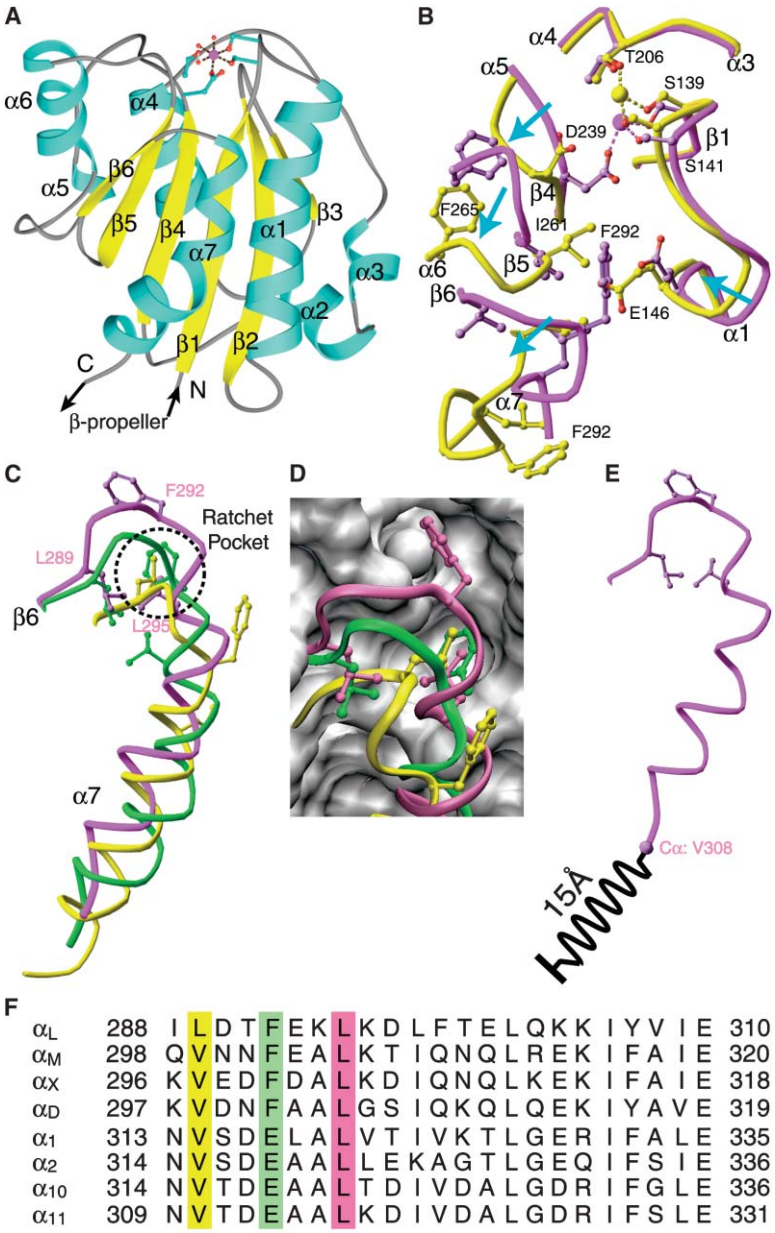

Figure 2. I Domain Structure and Activation

(A) Ribbon diagram of the α_L I domain in the closed conformation. The six β strands (yellow), seven α helices (cyan), and the N and C termini are labeled. The MIDAS metal ion (magenta sphere), side chains, and the oxygen atoms of three water molecules are shown in ball and stick models with oxygens shown in red. All ribbon diagrams are drawn with Ribbons (Carson, 1987).

(B) View of the top of the αL I domain including the MIDAS α1-β1, α3-α4, and β4-α5 loops. The closed and open Cα trace, key side chains shown in ball and stick models, and MIDAS metal ions shown as large spheres are shown in magenta and yellow, respectively; oxygens are shown in red. Primary coordinations are shown as dashed lines. Blue arrows show the direction of conformational movements.

(C and D) The three conformations of the β6-α7 loop. The Cα trace and ratchet side chains in ball-and-stick are shown in magenta, closed; green, intermediate; and yellow, open. (C) Overall view including the α7 helix. (D) Detail of the hydrophobic ratchet, with the interacting molecular surface shown in gray drawn with VMD (Humphrey et al., 1996).

(E) Schematic of the spring attached to the end of the α7 helix.

(F) Alignment of human I domain sequences, with the β6-α7 loop, the α7 helix, and the linker of the β propeller up to the conserved Glu residue. Residues that occupy the hydrophobic ratchet pocket in the open, intermediate, and closed conformations are highlighted in yellow, green, and magenta, respectively.

ranged from 0 to 1500 pN and decreased thereafter according to Hooke's law. Displacements of one and two turns of helix in the intermediate and open structures correspond to ~4 and ~8 Å, respectively; the distance of 15 Å was chosen so as not to bias to either the intermediate or the open structures. Thus, the intermediate or open structures would only be stabilized if they were at low-energy minima along the conformational pathway induced by displacement of the α7 helix in the axial, C-terminal direction, and if these states therefore resisted further α7 helix displacement. The simulations essentially converged in 100 ps (see "Time Course of Conformational Changes"). Therefore, the "end state" of each simulation was taken as the average of the structures saved every ps between 91 and 100 ps.

The end states were clustered as described in the Experimental Procedures (Figure 3). The average spring constant, α7 helix displacement, and final applied force are shown (Figure 3). Furthermore, comparisons between the average end state of all simulations in each cluster and crystal structures are shown for key conformational measures (Figure 3). The movement of the metal ion as it shifts 2 Å between the closed and open coordination states of the MIDAS was quantitated in simulations as the distance of the metal ion from its position in closed and open crystal structures. The ratchet position of the β6-α7 loop was quantitated as the distance of the C_β atoms of α_L residues Leu-295, Phe-292, and Leu-289 or the equivalent residues in other I domains from their position in the closed, intermediate, and open crystal structures, respectively, in which they occupy similar positions in the hydrophobic pocket. Fi-

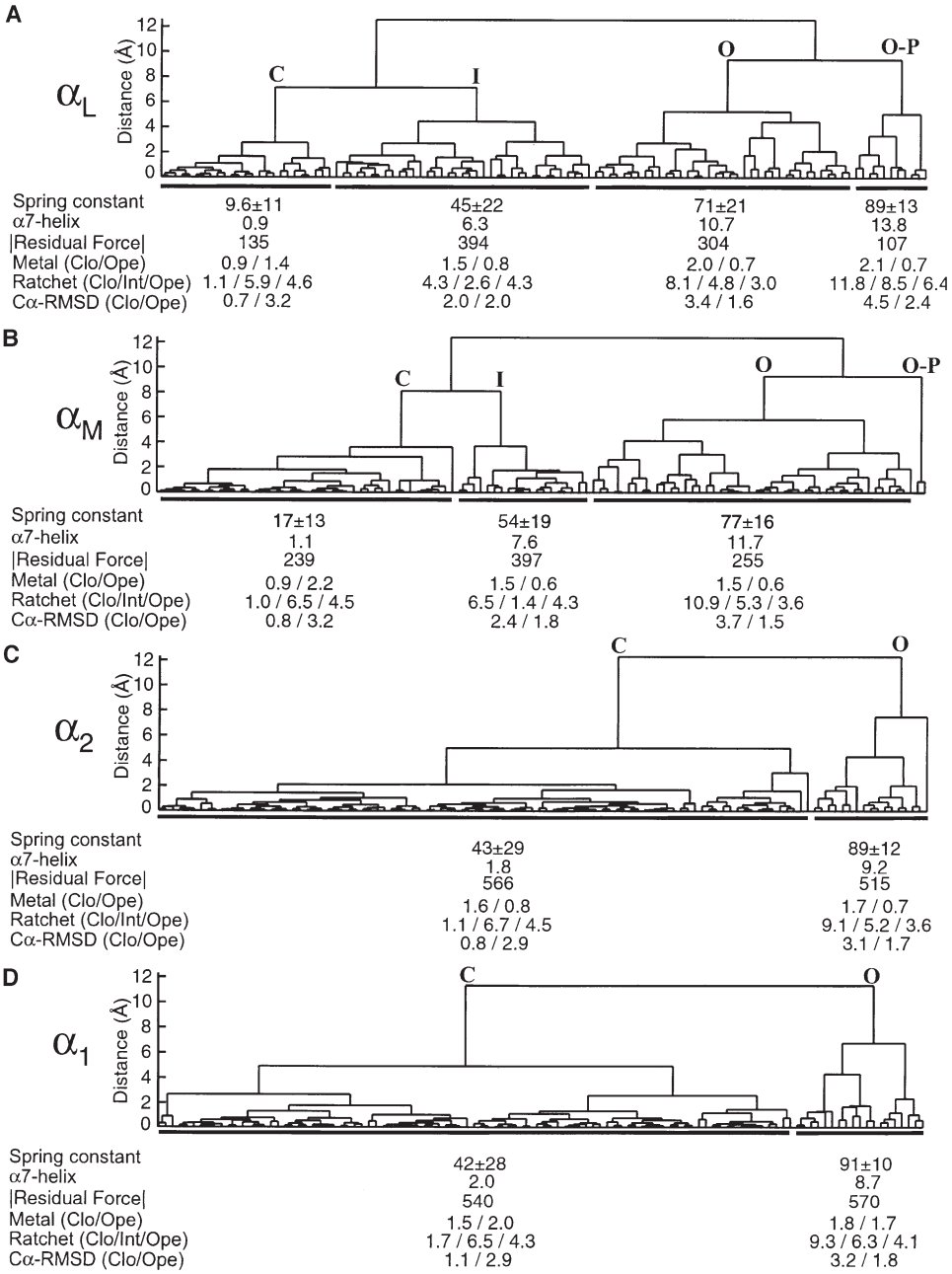

Figure 3. The Simulation End State Clusters

Branch length distances are shown in angstroms; note that a uniform distance between 6 and 9 Å is used to define the clusters for each I domain. The symbols "C," "I," "O," and "O-P" represent closed, intermediate, open, and overpulled clusters, respectively. The average ± SD spring constant and measurements for the average structure of all simulation end states in each cluster are shown below. The measurements are defined in Results. Differences are shown for closed (Clo), intermediate (Int), and open (Ope) crystal structures or for α7 helix structure models (see the Experimental Procedures).

nally, the rms deviation was determined for all Cα atoms with the closed and open structures.

The Three Discrete Conformations of the α_L I Domain

Simulations with the α_L I domain yielded four clusters that represent outcomes with progressively increasing spring constants (Figure 3A). The cluster with the lowest applied force (Cluster C, force constant = 9.6 ± 11 pN/Å) corresponds to the closed conformation, as shown by its α7 helix displacement, the match to the closed ratchet position, and its overall rmsd with the closed and open conformations. Inspection of the average structure of Cluster C showed little displacement of the hydrophobic side chains in the β6-α7 loop, Leu-289, Phe-292, and Leu-295 from their positions in the closed crystal structure (Figures 4A and 4B), despite the force remaining at the end state of 135 pN. Furthermore, the MIDAS loops

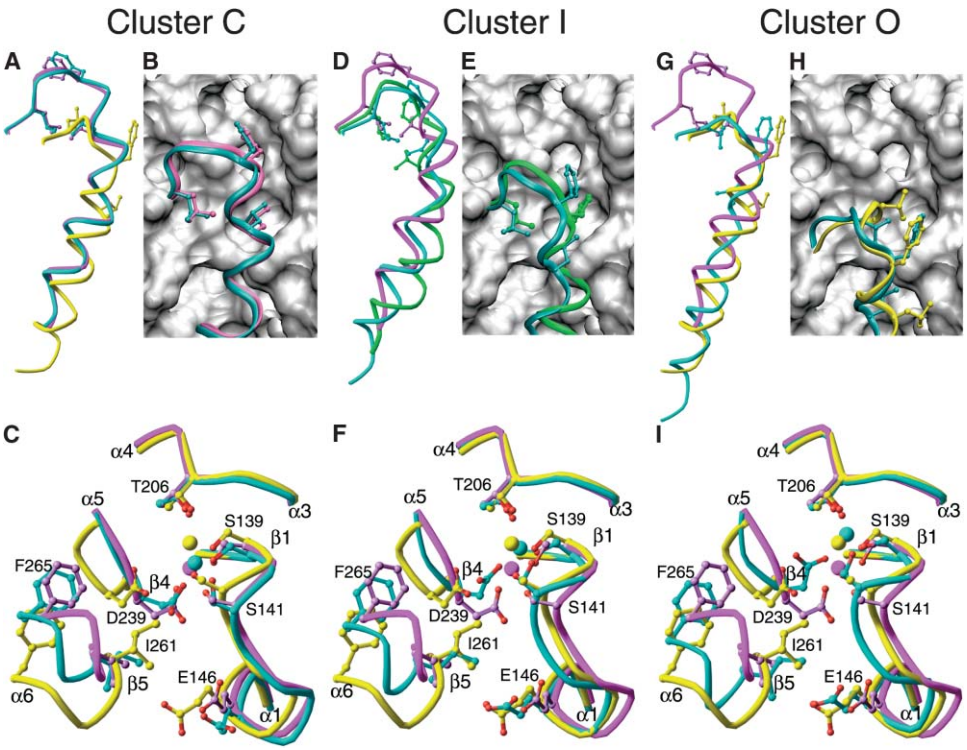

Figure 4. Comparison of Average α_L I Domain Simulation End States with Structures

(A–I) Closed (magenta), open (yellow), or intermediate (green) structures are compared to the average structure of the simulation end states (cyan) for (A–C) Cluster C, (D–F) I, and (G–I) O. (A, D, and G) β6-α7 loop and α7 helix. (B, E, and H) Details of the ratchet with the β6-α7 loop ribbon and interacting molecular surface. (C, F, and I) Loops around the MIDAS. See Figure 2 for details. All cluster backbone and Cβ atoms are of the average simulation end state structures. Since averaging can create stereochemical distortions, particularly in side chains, the remaining side chain atoms of the average simulation end state structures were subjected to energy minimization (100 steps of steepest descent).

and the metal ion remained in their closed conformation (Figure 3A and 4C), and the β5-α6 loop and its Phe-265 side chain, which moves to allow flipping of the β4-α5 loop in MIDAS rearrangement, remained near their positions in the closed structure (Figure 4C).

Clustering showed that of the 110 α_L I domain simulations, 37 (or 34%) adopted the intermediate conformation of the β6-α7 loop (Cluster I, Figure 3A). This cluster was obtained at an intermediate force constant regime of 45 ± 22 pN/Å. The position of the β6-α7 ratchet residue in the hydrophobic pocket was closest to that of the intermediate crystal structure for Cluster I, with a distance of 2.6 Å from the intermediate ratchet position compared to 4.3 Å from both the closed and open ratchet positions. The position of the metal ion was closer to that of the open conformation (0.8 Å) than that of the closed conformation (1.5 Å). This metal position contrasts with the intermediate α_L I domain crystal structure (see Discussion).

In the average structure of Cluster I, compared to the closed structure, Phe-292 has moved out of its upper pocket and has replaced Leu-295 in the ratchet pocket (Figures 4D and 4E). The position of the β6-α7 loop was slightly lower and more outward than in the intermediate crystal structure, and this position reflects the greater displacement of the α7 helix centroid of 6.3 Å compared to 4 Å in the intermediate model structure. The downward movement of Phe-292 induced a rearrangement of neighboring residues, including the β1-α1 and β4-α5 loops bearing MIDAS residues and the β5-α6 loop (Figure 4F). Consistent with the movement of the metal ion toward the open position, the rearrangements around the MIDAS were overall very similar to those seen in open compared to closed crystal structures (Figure 4F). For example, the α1 helix moved inward toward the hydrophobic core of the domain and filled with the side chain of Glu-146 some of the space vacated by Phe-292 in the upper pocket (Figure 4F). The inward movement of the α1 helix was linked to the shift in position of the β1-α1 loop containing Ser residues 139 and 141 of the MIDAS DXSXS motif. These Ser side chains and the metal moved closer to Thr-206, with formation of the direct metal coordination bond to Thr-206 observed in the open, but not closed, MIDAS conformation (Figure 4F).

One cluster of α_L simulations attained a β6-α7 loop conformation with a ratchet position much closer to that of the open crystal structure (3.0 Å) than the closed or intermediate structures (8.1 and 4.8 Å, respectively) and was therefore designated Cluster O (Figure 3A). Cluster O was attained at a higher spring constant than Cluster I, and the downward displacement of the α7 helix centroid of 10.7 Å was also greater than in Cluster I and similar to the α7 helix displacement in open crystal

structures of 8 Å. The MIDAS metal ion was within 0.7 Å and 2.0 Å of its position in the open and closed structures, respectively. The average structure of Cluster O confirmed that the β6-α7 loop and MIDAS region were in the open conformation (Figures 4G–4I). The average Cluster O simulation adopted α1 helix and β1-α1 loop conformations similar to those of the average Cluster I simulation and open crystal structures (Figure 4I). Compared to Cluster I, the Cluster O average structure attained conformations of the β4-α5 and β5-α6 loops more similar to those seen in the open α_L crystal structure. In the closed to open transition, there is a remarkable flip in the backbone angle of Gly-240 in the β4-α5 loop (Lee et al., 1995a; Shimaoka et al., 2003). A partial flip of the β4-α5 loop also occurred in cluster O simulations (Figure 4I). Despite the partial reproduction of this flip, there was divergence in the position of the side chain of MIDAS residue Asp-239 in the β4-α5 loop between simulation and structure, emphasizing the importance of packing interactions over Asp-239 metal coordination in driving this β4-α5 loop movement.

The cluster formed at the highest force regime of 89 ± 13 pN/Å was designated O-P for overpulled, because the α7 helix was pulled beyond the position observed in the open conformation (Figure 3A). The β6-α7 loop conformation also differed from that observed in any crystal structures. Therefore, the O-P cluster appears to represent a non-native state resulting from application of excessive force and was not studied further.

Time Course of Conformational Changes

The time course of conformational change was calculated for each cluster by averaging each picosecond the absolute displacements for the previously described conformational markers (Figure 5). This is of particular interest to determine whether the intermediate conformation is on the pathway from the closed to the open conformation. Most change occurred within the first 10 ps of simulations, with more gradual change occurring thereafter (Figure 5). The Mg^{2+} ion position was unchanged over the time course of Cluster C simulations, whereas it moved toward the open position in the Cluster I and O simulations (Figure 5A). When the metal moved to within less than 1 Å of its position in the open conformation, the direct coordination to the side chain Oγ atom of Thr-206 characteristic of the open coordination state was invariably observed. The final position of the MIDAS Mg^{2+} ion was close to its position seen in the open crystal structure, and this position was reached after ~50 ps (Figure 5A).

Displacement of the Cβ atom of residue 295 from the hydrophobic ratchet pocket occurred in Clusters I and O, but not C (Figure 5B). This residue is present within the first turn of the α7 helix, and the rate and extent of its displacement in Clusters I and O thus closely mirror the downward movement of the α7 helix (Figure 5B).

Comparison of the position of the Cβ atom of Phe-292 to its position in the hydrophobic detent pocket of the intermediate α_L crystal structure showed that Cluster I simulations first exhibited a displacement of Phe-292 from its position in the closed structure and approached the hydrophobic ratchet pocket within ~4 Å at 20 ps

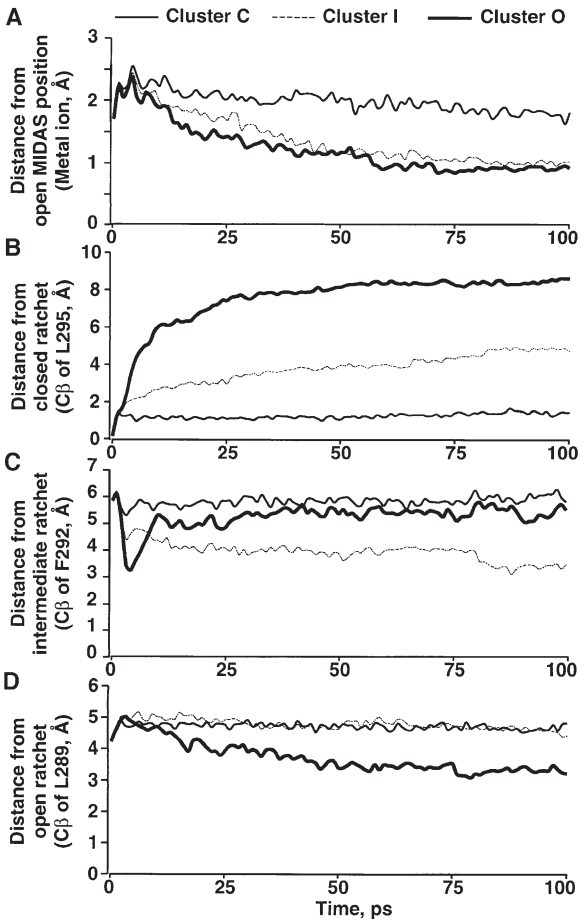

Figure 5. Simulation Time Courses

Shown are the same distance measures between simulations and structures as described in Results. To show the robustness of the results, here we show the average of the distances of all simulations in each cluster from the structure, whereas in Figures 3 and 6, the distance of the average simulation end state from the structure is shown.

(Figure 5C); then, at ~80 ps, it achieved a stable position within this pocket. Most interestingly, Cluster O simulations reached the intermediate conformation of the β6-α7 loop with Phe-292 in the intermediate ratchet position at ~5 ps (Figure 5C). At this time point in Cluster O simulations, Phe-292 was as close to the intermediate ratchet position as it was at the end state of Cluster I simulations (Figure 5C). Cluster O simulations reached the open conformation of the β6-α7 loop with Leu-289 in the detent position after approximately 50 ps, and Leu-289 initially moved away from this position at 5 ps (Figure 5D). The initial movements up to 5 ps of Phe-292 and Leu-289 in Cluster O indicate that the intermediate conformation of the β6-α7 loop is on the pathway of conformational change from the closed to the open conformation.

Clustering of Simulation End States in α_M, α_2, and α_1 I Domains

Sequence alignment of integrin I domains shows interesting properties of the residues found at the three

ratchet positions (Figure 2F). Leu is invariant at the position that occupies the pocket in the closed ratchet position, e.g., Leu-295 in α_L (Figure 1F and not shown for other vertebrate I domains). The residue that occupies the ratchet pocket in the open position is Val in all I domains except α_L, where it is Leu (Leu-289), both in mouse and human (Figure 1F and data not shown). The residue in the intermediate ratchet position, i.e., Phe-292 in α_L, is Phe in the α_L, α_M, α_X, and α_D subunits that associate with the β_2 subunit, Tyr in α_E, and Glu in the collagen binding α_1, α_2, α_{10}, and α_{11} subunits that associate with the β_1 subunit (Figure 1F and data not shown). The Glu residue forms a salt bridge to Arg-288 in the β5-α6 loop in the α_2 I domain in the closed, but not open, conformation (Emsley et al., 2000), and it would not be expected to occupy the hydrophobic ratchet pocket in the intermediate β6-α7 conformation.

Among the α_M, α_1, and α_2 I domains, only the clusters of simulations with α_M were similar to those of α_L (Figure 3B). The ratchet positions of α_M Clusters C, I, and O clearly demonstrated the adoption of closed, intermediate, and open positions, respectively, of the β6-α7 loop, and the open MIDAS conformation was achieved in Clusters I and O (Figure 3B). Furthermore, the overall rmsd of Clusters C and O were closest to the closed and open crystal structures, respectively, whereas that of Cluster I was intermediate. In contrast to α_L simulations, Cluster I was only half as populated in α_M (Figures 3A and 3B).

The simulation results with α_1 and α_2 were similar in regard to the β6-α7 conformation and were distinct from α_L and α_M. Cluster C was far more populated in α_1 and α_2 simulations (83% and 85%, respectively) than in α_L and α_M simulations (23% and 38%, respectively) (Figure 3). Cluster O was more abundant in α_L and α_M I domain simulations (34% and 42%, respectively) than in α_1 and α_2 simulations (17% and 15%, respectively). Remarkably, intermediate clusters were not formed in α_1 and α_2 simulations (Figures 3C and 3D). Visual inspections of simulation trajectories revealed that the β6-α7 loop moved directly to the open position once the Arg salt bridge to the Glu in the ratchet was broken. Regarding the MIDAS conformation, the position of the metal ion shifted closer to the open position in Cluster O than in C for both α_1 and α_2 I domains; however, simulation of MIDAS movement was markedly less robust than for α_L and α_M I domains.

Discussion

It is hypothesized that in an intact integrin heterodimer, forces applied at interdomain boundaries could change the affinity of the ligand binding site of the I domain. We have used molecular dynamics to simulate the application of force to the I domain at its C-terminal α7 helix to test whether this could induce the intermediate and open conformations, which have intermediate and high affinity for ligand, respectively. Furthermore, we wished to learn whether the intermediate conformation of the β6-α7 loop was on the pathway to the open conformation, whether the intermediate conformation would be stable in the wild-type sequence in a particular force constant regime, and whether the intermediate conformation might be stable for I domains other than when it is constrained by a mutationally introduced disulfide in the integrin α_L subunit, for which the only example exists of a crystal structure (Shimaoka et al., 2003).

We wished to test whether we could reproduce intermediate and open conformations seen in crystal structures by applying a C-terminal pull spring in molecular dynamic simulations. Therefore, we did not explicitly favor a particular crystallographic end state, as is commonly done in many molecular dynamic simulations (e.g., biased or targeted molecular dynamics [Paci and Karplus, 1999; Ma et al., 2002]) in which the main point is to determine a representative pathway and path-dependent thermodynamic properties between two crystallographic states. In contrast, in our simulation, the external pulling force (to mimic a physiological case) alters the underlying potential energy surface of the molecule, therefore "tilting" the mimina toward new, distinct conformations; these are the intermediates we are interested in finding, and we seek to simulate the relaxation to these new equilibrium points.

Furthermore, we carried out a large number of simulations at varying forces, and we clustered the resulting end states to ensure that the data are representative of the most frequent stochastic events as well as the range of possible outcomes. Clustering allowed us to structurally group, classify, and quantify the simulation outcomes, to correlate the outcome with the applied force, and to make comparisons among different I domains. The results with Cluster O demonstrated that an open conformation of the α_L and α_M I domains was induced by the applied force on the α7 helix that resembled that seen in crystal structures in many important respects. The α1 helix moved inward, and the β1-α1 loop containing two serine residues coordinating the Mg^{2+} ion moved into its position in the high-affinity, open conformation. The Mg^{2+} ion moved about 2 Å and formed the coordination to Thr-206 paradigmatic of the open conformation. Furthermore, the β4-α5 loop underwent a partial flip near Gly-240, and the β5-α6 loop shifted toward its position in the open structure. Moreover, the β6-α7 loop, which is not part of the ligand binding site but is crucial for linking the motion of the α7 helix to the MIDAS (Shimaoka et al., 2003), adopted the conformation typical of the open conformation. These results demonstrate that the open conformation of the integrin I domain can be induced by downward movement of the α7 helix, confirming a recent crystal structure of a mutant, high-affinity I domain in the open conformation in the absence of a bound ligand or ligand mimetic (Shimaoka et al., 2003).

Despite some notable successes in this study, it is important to point out limitations and deficiencies. We did not impose any restraints on conformational movements in the I domain, except for applying a force on the α7 helix; however, regions that were known not to undergo significant movement were harmonically constrained to prevent nonphysiologic rearrangements (see the Experimental Procedures). This approach allowed us to mimic a physical interaction on the simulation time scale and to obtain meaningful results with an approximate treatment of the solvent and the neglect of other

domains in the integrin. Although β6-α7 loop movements appeared to be robustly simulated in α_1 and α_2 I domains, these movements did not correlate with MIDAS metal ion movements. In α_1 and α_2 I domains compared to α_L and α_M, an extra helix is inserted in the β5-α6 loop, which undergoes significant reshaping in the open conformation (Emsley et al., 2000). The α_1 and α_2 MIDAS simulations may reflect the difficulty of simulating a longer relaxation event caused by the larger number of residues that shift in conformation around the α_1 and α_2 MIDAS compared to the α_L and α_M MIDAS. Alternatively, communication between the β6-α7 loop and MIDAS may differ in α_1 and α_2 I domains and α_L and α_M I domains. The shift to the open conformation has been demonstrated upon ligand binding for this subset of I domains (Emsley et al., 2000), but whether the MIDAS shifts upon α7 helix displacement alone has not yet been tested. Furthermore, an antibody bound to the α_1 MIDAS induces a shift to the open MIDAS without a corresponding β6-α7 loop shift (Karpusas et al., 2003).

One of the most important results of this study is the validation by Cluster I of the intermediate conformational state of the β6-α7 loop of the I domain. Not only was the intermediate conformation of the β6-α7 loop attained as the end state in Cluster I, but it was also on the pathway of conformational change to the open conformation of the β6-α7 loop in Cluster O. Thus far, the only intermediate conformation crystal structure comes from a disulfide-linked mutant of the α_L I domain (Shimaoka et al., 2003); however, an intermediate conformational state with intermediate affinity for ligand is hypothesized to be important for fine tuning of adhesiveness through $\alpha_L\beta_2$, and to account for the observation of increased adhesiveness through $\alpha_L\beta_2$ in the absence of detectable high affinity for soluble ligand (Shimaoka et al., 2001, 2003). A large proportion of α_L I domain simulations attained an intermediate position of the β6-α7 loop with Phe-292 in the ratchet pocket. Furthermore, Cluster I withstood a greater residual force on the α7 helix (394 pN) than either Cluster C (135 pN) or Cluster O (304 pN). These findings demonstrate that the intermediate conformation of the β6-α7 loop is at an energy minimum over a wide range of forces applied to the I domain C-terminal α helix. Therefore, our results provide strong support for the previous proposal that the intermediate conformation of the β6-α7 loop is not a crystal or mutational artifact and could be of physiologic importance for fine regulation of integrin affinity, particularly for $\alpha_L\beta_2$. Interestingly, three different overall conformational states of integrin heterodimers have been demonstrated by electron microscopy (Takagi et al., 2002); however, there is no evidence for or against a one-to-one correspondence with I domain conformational states.

In an interesting contrast, the mutant, intermediate-affinity α_L I domain crystallized with its β6-α7 loop in the intermediate conformation and its MIDAS in the closed conformation (Shimaoka et al., 2003), whereas, in Cluster I simulations, the β6-α7 loop was in the intermediate conformation and the MIDAS was in the open conformation. It is possible that this reflects inadequate simulation of the MIDAS; however, a more interesting possibility is that the simulations better reflect the state of the MIDAS in solution. The kinetics of binding to ICAM-1 have been measured with high-affinity and intermediate-affinity mutants and wild-type α_L I domains (Shimaoka et al., 2003). These demonstrate that the high- and intermediate-affinity I domain mutants have indistinguishable on-rates of $115 \pm 7 \times 10^3$ $M^{-1}s^{-1}$ and $133 \pm 10 \times 10^3$ $M^{-1}s^{-1}$, compared to $3.1 \pm 0.1 \times 10^3$ $M^{-1}s^{-1}$ for the wild-type, closed I domain (Shimaoka et al., 2003). These on-rates suggest that the open, ligand bound conformation of the MIDAS predominates in solution for both the high- and intermediate-affinity I domains. The off-rates are 0.014, 0.43, and 4.6 s^{-1}, for the high-affinity, intermediate-affinity, and wild-type I domains, respectively. The off-rates are consistent with the open MIDAS conformation being more stable with the open conformation than the intermediate conformation of the β6-α7 loop.

Clustering of simulations revealed interesting differences among I domains. The closed conformation was markedly more stable in the α_1 and α_2 I domains than in α_L and α_M, based on the high residual force it withstood at the end of simulations (Figure 3) and the high proportion of Cluster C and lack of Cluster I simulations for α_1 and α_2 I domains. This appeared to be a consequence of the Arg-Glu salt bridge that stabilizes the closed conformation in α_1 and α_2 and the unfavorable energetics of placing the Glu in the intermediate position in the hydrophobic ratchet pocket.

Because α_L and α_M share a Phe residue at the intermediate ratchet position compared to the Glu residue in α_1 and α_2 at this position, we initially expected that the distribution of conformational states would be similar in α_L and α_M, similar in α_1 and α_2, and distinct when α_L and α_M were compared to α_1 and α_2. Indeed, the closed state is much more populated in α_1 and α_2 simulations than in α_L and α_M, and the intermediate state is absent in α_1 and α_2 simulations. However, an unexpected insight is that the intermediate state is twice as populated in α_L as in α_M. This is most interesting, because there is extensive evidence for α_L, but not yet for α_M, that it can become activated for binding to ICAM-1 in the absence of attaining high affinity for ICAM-1 (Carman and Springer, 2003). Furthermore, the intermediate conformation of the β6-α7 loop has been structurally demonstrated for α_L, but not yet for any other I domain (Shimaoka et al., 2003).

Seeking to explain the greater propensity of α_L than α_M for the intermediate conformation of the β6-α7 loop, we noted that α_L contains a Leu as the first of the three ratchet residues, whereas all of the other eight vertebrate I domains contain Val, with one less methylene group, in this position (Figure 2F). In the closed and intermediate conformations, Leu-289 is buried in a hydrophobic pocket adjacent to the ratchet pocket. Leu-289 must be removed from this pocket and moved to the ratchet pocket in the transition from the intermediate to the open conformation. Molecular dynamics of mutant α_L and α_M I domains indeed confirmed that the presence of Leu in this position strikingly influences the stability of the intermediate conformation of the β6-α7 loop (Figure 6). The mutation of Val to Leu in α_M increased the population of the intermediate cluster, from 19 to 30, and decreased the population of the open cluster, from 46 to 24 (Figure 3B and 6B). The effect of mutation of the first ratchet residue was even more dramatic in the

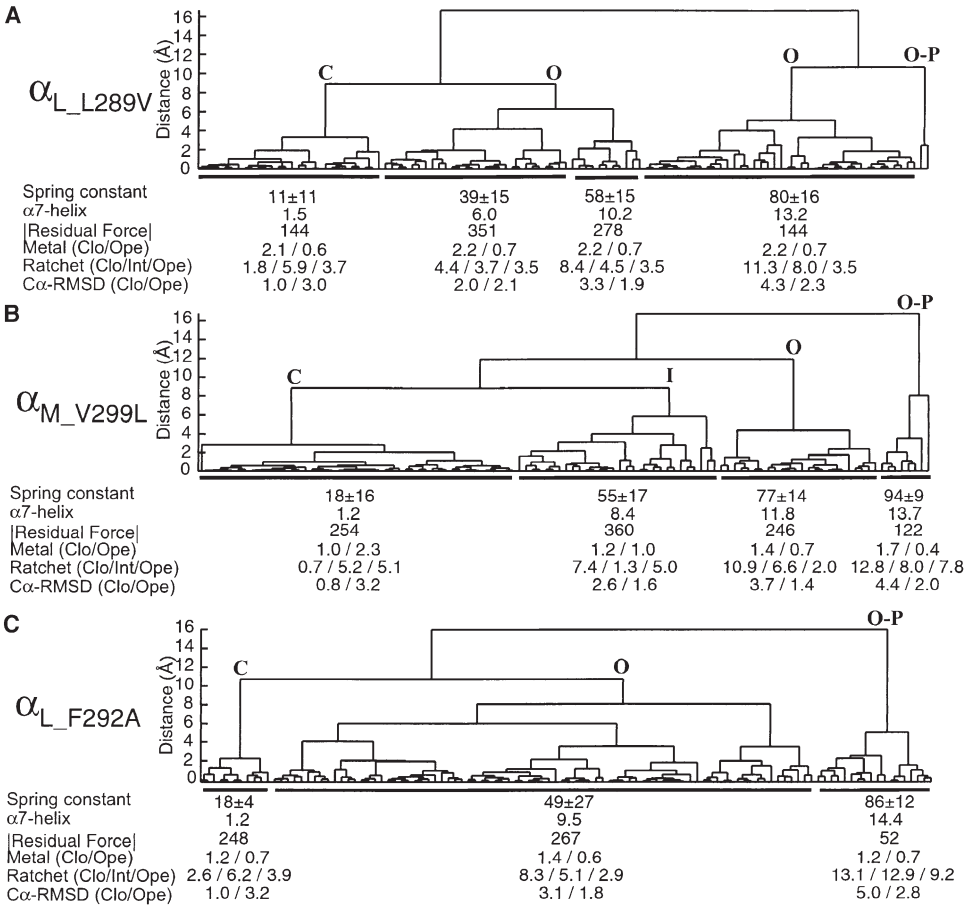

Figure 6. The Mutant Simulation End State Clusters

Simulations and measurements are exactly as for wild-type in Figure 3, but they began with the energy-minimized structure (see the Experimental Procedures) with the indicated mutations.

Leu to Val mutation in α_L. Despite the overall similarity in the clustering patterns (Figure 3A compared to Figure 6A), none of the L289V α_L clusters attained a true intermediate state, as shown by the positions of the three hydrophobic ratchet residues (Figure 6A). Another interesting observation was that the L289V mutant adopted the open MIDAS even in Cluster C (Figure 6A). Visual inspection of each simulation in the closed cluster revealed that the L289V mutation allowed for separation of the β6-α7 loop from the body of the domain, as well as inward motion of the α1 helix and opening of the MIDAS in the absence of downward α7 helix displacement.

The intermediate ratchet position Phe residue is buried in both the closed and intermediate conformations, and it is exposed in the open conformation (Lee et al., 1995a; Shimaoka et al., 2003). The F292A mutation in α_L dramatically decreased the population of Cluster C, increased the population of Cluster O, and eliminated Cluster I (Figure 6C). Thus, mutation of this residue is highly activating, as has been previously suggested based on experimental evidence for α_M (Li et al., 1998).

In summary, molecular dynamics has allowed us to confirm that an experimentally observed intermediate conformational state of the α_L I domain is at a low-energy minimum over a wide range of applied forces on the α7 helix and is on the pathway of conformational change to the open conformation. Furthermore, the studies have provided insights into differences among I domains in the relative stabilities of the three conformational states. Ratchet residues emerge as key regulators of the stabilities of these states, and thus this study has provided new experimentally testable hypotheses.

Experimental Procedures

I Domain Coordinates Files

All molecular dynamic simulations were done with I domain structures in the closed conformation, and for comparison among α_L, α_M, α_1, and α_2 I domains, the coordinate files began and ended with residues in equivalent positions. The closed crystal structures were for α_M, PDB code 1JLM (Lee et al., 1995a), residues 132–318; for α_1, PDB code 1QC5 (Rich et al., 1999), residues 32–221 (142–331 in mature sequence); and for α_2, PDB code 1AOX (Emsley, et al., 1997), residues 143–334. Because closed α_L crystal structures differ from one another in the α7 helix due to unusual crystal packing interactions, the α_L model used residues 129–292 of the high-resolution structure 1LFA (Qu and Leahy, 1995) together with α7 helix residues 293–308 of 1ZON (Qu and Leahy, 1996), which has an α7 helix more typical of other I domains, after superposition with residues 129–139, 157–190, 204–227, 232–238, 242–261, and 273–292. The MIDAS Mg^{2+} ion and three explicit water molecules present in the primary coordination shell of the Mg^{2+} ion were included in all closed coordinate files. When necessary, these were added by replacing atoms

in identical positions, e.g., a Mn^{2+} with Mg^{2+} in 1JLM and a Cl^- with a water in 1LFA.

Coordinate files for intermediate and open structures were used only for comparison to and clustering of the simulations. Models were required for the C-terminal portion of the α7 helix, which is disordered in open crystal structures, and for the α7 helix in intermediate and open wild-type α_L I domains, in which it is disrupted by the mutationally introduced disulfide bonds. The open α_M model used residues 132–315 of 1IDO (Lee et al., 1995b); residues 316–318 were modeled from 1JLM (Lee et al., 1995a) after superimposing residues 308–315. The open α_L model used residues 129–289 of the open structure, PDB code 1MQ9 (Shimaoka et al., 2003). Residues 290–308 were modeled on residues 303–318 of the open α_M model after superimposing α_M residues 150–163, 266–271, and 294–301 onto 1MQ9 residues 147–160, 256–261, and 284–291. The intermediate α_L model used residues 129–292 from the intermediate structure, PDB code 1MJN (Shimaoka et al., 2003). Residues 293–308 were modeled from residues 303–318 of the open α_M model described above, after superimposing α_M residues 303–316 on 1MJN residues 293–306. The open α_2 model used residues 143–323 of 1DZI (Emsley et al., 2000); residues 324–334 were modeled on residues 308–318 of the open α_M model after superimposing open α_M residues 134–139, 153–160, 168–179, 234–238, and 293–302 onto 1DZI residues 145–150, 162–169, 179–190, 246–250, and 309–318.

For comparisons between crystal structures and simulations, all I domain closed, intermediate, and open structures and models were aligned by superposition onto the closed α_L structure. The residues that were used for superimposing onto the closed αL I domains (the residue position for α_L is within parentheses) for α_M were: 132–162 (129–159), 171–188 (168–185), 204–222 (201–219), 233–245 (230–242), 265–271 (255–261), 288–304 (278–294); and for α_2 (and equivalent positions for α_1) were 143–155 (129–137), 162–170 (150–158), 181–196 (167–182), 221–257 (206–242), 274–281 (253–260), 303–334 (277–308). Then, open I domains of α_L, α_M, and α_2 were superimposed onto the corresponding closed I domains by using the following residues: for α_L: 129–140, 164–181, and 231–237; for α_M: 132–177, 180–240, 257–268, 290–294; and for α_2: 143–151, 166–199, 203–216, 224–253, 267–279. The intermediate α_L I domains were superimposed onto closed α_L I domains by using residues 129–136, 168–195, 202–220, 227–231, 235–239, 249–258, and 271–279. The coordinates of the intermediate ratchet were determined from the Cβ of Phe-292 of the intermediate α_L structure for all of the I domains after superposition as described above. The coordinates of Cα atoms, ratchet Cβ atoms, and the MIDAS metal ion of the α_1 open I domain were approximated as being identical to those in the α_2 open I domain. There are no insertions/deletions between these two domains.

Simulations

Molecular dynamics and energy minimization were run by using the CHARMM software package (Brooks et al., 1983) with version 19 force field parameters, with the following additional parameters for the Mg^{2+} ion: charge, +2; radius, 1.185; relative weight, 24.3; and the EEF1 implicit solvent model (Lazaridis and Karplus, 1999). Three water molecules occupy specific positions in the Mg^{2+} coordination shell, and two of these are buried. We found that the use of explicit water molecules in these positions improved simulations. Thus, with implicit solvent only, after energy minimization and 10 ps of molecular dynamics equilibration as described below, the Mg^{2+} ion shifted 0.8 Å from its initial position in the closed crystal structures. However, when these explicit water molecules were added, the Mg^{2+} ion remained within 0.25 Å of its initial position. The partial charges of the water molecules in TIP3 (Jorgensen et al., 1983) were originally developed for simulating the effect of bulk and explicit water molecules. Since in our simulations two of the explicitly modeled waters were buried, and the effect of explicit water molecules was simulated within an implicit solvation model, the partial charges of TIP3 needed to be adjusted from −0.834 and 0.417 to −0.2 and 0.1 for oxygen and hydrogen atoms, respectively. The oxygen atoms of the three water molecules were weakly harmonically constrained with a force constant of 10 × [atomic mass] pN/Å, which kept them in the vicinity of the Mg^{2+} ion.

Coordination between Mg^{2+} and carbonyl oxygens is highly unfavorable (Harding, 2001). To prevent such spurious coordinations, the partial charges of the carbonyl groups of residues 139–141, residue 239 in the α_L I domain, and the corresponding residues in other I domains were adjusted from −0.55 and 0.55 to −0.15 and 0.15 for carbonyl oxygen and carbon atoms, respectively.

After the initial atomic coordinates of all I domains were obtained (see above), they were subjected to energy minimization with 1,000 steps of the Steepest Descent method, followed by 10 ps of molecular dynamics at 300 K, with the backbone atoms of structurally conserved regions (see below) constrained harmonically. The spring was attached to the Cα atom of the C-terminal residue of the α I domain and was stretched 15 Å to a fixed point along the projection of the α7 helical axis (Figure 2E). The spring constant was varied in ~10 pN/Å increments. Independence among the ten simulations at ~10 pN/Å increments was insured by small variations of −0.8, −0.6, −0.4, −0.2, 0, 0.2, 0.4, 0.6, 0.8, and 1.0 pN/Å. For example, for the ten simulations at nominally 10 pN/Å, one simulation was done at each of 9.2, 9.4, 9.6, 9.8, 10.0, 10.2, 10.4, 10.6, 10.8, and 11.0 pN/Å, and the spring constant was held constant during each of these. To distribute the force applied to the single atom over the last portion of the α7 helix, the backbone dihedral angles of the last 12 residues were harmonically constrained to be close to their angles in their initial, helical conformation.

Once the spring force was applied, the backbone atoms whose coordinates in the closed and open structures are similar, i.e., displaced less than 0.5 Å, and are not part of the MIDAS, were harmonically constrained with a force constant of 140 × [atomic mass] pN/Å; this allowed the constrained atoms to fluctuate by about 0.5 Å relative to their initial positions. The residues under harmonic constraint were as follows: for α_L, 129–138, 150–160, 165–203, 203–238, 244–256, and 279–280; for α_M, 132–141, 152–163, 168–206, 211–241, 248–266, and 289–290; and for α_2 (and equivalent residues for α_1), 143–152, 161–172, 179–215, 223–253, 259–277, and 305–306. The CHARMM input file is shown in the Supplemental Data.

Clustering

The average distances were determined between each simulation end state and the closed, intermediate, and open structures for the Cβ atoms of the three ratchet residues, i.e., Leu-295, Phe-292, and Leu-289, respectively, and the α7 helix centroid that was defined by the mean coordinates of the last 12 Cα atoms. The simulations were then clustered hierarchically (complete linkage clustering) with the software MATLAB by using the average of the four distances to each of the three crystal structures.

Supplemental Data

Supplemental data including CHARMM input files (idomain_pull.inp) and topology/parameter files (toph19_eef1_mod.inp; param19_eef1_mod.inp) are available at http://www.structure.org/cgi/content/full/12/12/2137/DC1/.

Acknowledgments

This work was supported by National Institutes of Health grants CA31798 and HL48675. We deeply appreciate contributions from Martin Karplus to this work.

Received: June 22, 2004
Revised: September 10, 2004
Accepted: October 5, 2004
Published: December 7, 2004

References

Alonso, J.L., Essafi, M., Xiong, J.P., Stehle, T., and Arnaout, M.A. (2002). Does the integrin αA domain act as a ligand for its βA domain? Curr. Biol. *12*, R340–R342.

Brooks, B.R., Bruccoleri, R.E., Olafson, B.D., States, D.J., Swaminathan, S., and Karplus, M. (1983). CHARMM: a program for macromolecular energy, minimization, and dynamics calculations. J. Comp. Chem. *4*, 187–217.

Carman, C.V., and Springer, T.A. (2003). Integrin avidity regulation:

are changes in affinity and conformation underemphasized? Curr. Opin. Cell Biol. *15*, 547–556.

Carson, M. (1987). Ribbon models of macromolecules. J. Mol. Graph. *5*, 103–106.

Emsley, J., King, S.L., Bergelson, J.M., and Liddington, R.C. (1997). Crystal structure of the I domain from integrin α2b1. J. Biol. Chem. *272*, 28512–28517.

Emsley, J., Knight, C.G., Farndale, R.W., Barnes, M.J., and Liddington, R.C. (2000). Structural basis of collagen recognition by integrin $\alpha2\beta1$. Cell *101*, 47–56.

Harding, M.M. (2001). Geometry of metal-ligand interactions in proteins. Acta Crystallogr. D Biol. Crystallogr. *57*, 401–411.

Humphrey, W., Dalke, A., and Schulten, K. (1996). VMD: visual molecular dynamics. J. Mol. Graph. *14*, 33–38.

Huth, J.R., Olejniczak, E.T., Mendoza, R., Liang, H., Harris, E.A., Lupher, M.L., Jr., Wilson, A.E., Fesik, S.W., and Staunton, D.E. (2000). NMR and mutagenesis evidence for an I domain allosteric site that regulates lymphocyte function-associated antigen 1 ligand binding. Proc. Natl. Acad. Sci. USA *97*, 5231–5236.

Isralewitz, B., Gao, M., and Schulten, K. (2001). Steered molecular dynamics and mechanical functions of proteins. Curr. Opin. Struct. Biol. *11*, 224–230.

Jorgensen, W.L., Chandrasekhar, J., Madura, J.D., Impey, R.W., and Klein, M.L. (1983). Comparison of simple potential functions for simulating liquid water. J. Chem. Phys. *79*, 926–935.

Kallen, J., Welzenbach, K., Ramage, P., Geyl, D., Kriwacki, R., Legge, G., Cottens, S., Weitz-Schmidt, G., and Hommel, U. (1999). Structural basis for LFA-1 inhibition upon lovastatin binding to the CD11a I-domain. J. Mol. Biol. *292*, 1–9.

Karplus, M., and McCammon, J.A. (2002). Molecular dynamics simulations of biomolecules. Nat. Struct. Biol. *9*, 646–652.

Karpusas, M., Ferrant, J., Weinreb, P.H., Carmillo, A., Taylor, F.R., and Garber, E.A. (2003). Crystal structure of the $\alpha1\beta1$ integrin I domain in complex with an antibody fab fragment. J. Mol. Biol. *327*, 1031–1041.

Lazaridis, T., and Karplus, M. (1999). Effective energy function for proteins in solution. Proteins *35*, 133–152.

Lee, J.-O., Bankston, L.A., Arnaout, M.A., and Liddington, R.C. (1995a). Two conformations of the integrin A-domain (I-domain): a pathway for activation? Structure *3*, 1333–1340.

Lee, J.-O., Rieu, P., Arnaout, M.A., and Liddington, R. (1995b). Crystal structure of the A domain from the α subunit of integrin CR3 (CD11b/CD18). Cell *80*, 631–638.

Legge, G.B., Kriwacki, R.W., Chung, J., Hommel, U., Ramage, P., Case, D.A., Dyson, H.J., and Wright, P.E. (2000). NMR solution structure of the inserted domain of human leukocyte function associated antigen-1. J. Mol. Biol. *295*, 1251–1264.

Li, R., Rieu, P., Griffith, D.L., Scott, D., and Arnaout, M.A. (1998). Two functional states of the CD11b A-domain: correlations with key features of two Mn^{2+}-complexed crystal structures. J. Cell Biol. *143*, 1523–1534.

Lu, C., Shimaoka, M., Ferzly, M., Oxvig, C., Takagi, J., and Springer, T.A. (2001). An isolated, surface-expressed I domain of the integrin $\alpha L\beta2$ is sufficient for strong adhesive function when locked in the open conformation with a disulfide. Proc. Natl. Acad. Sci. USA *98*, 2387–2392.

Ma, J., Flynn, T.C., Cui, Q., Leslie, A.G., Walker, J.E., and Karplus, M. (2002). A dynamic analysis of the rotation mechanism for conformational change in F(1)-ATPase. Structure *10*, 921–931.

Paci, E., and Karplus, M. (1999). Forced unfolding of fibronectin type 3 modules: an analysis by biased molecular dynamics simulations. J. Mol. Biol. *288*, 441–459.

Qu, A., and Leahy, D.J. (1995). Crystal structure of the I-domain from the CD11a/CD18 (LFA-1, $\alpha_L\beta2$) integrin. Proc. Natl. Acad. Sci. USA *92*, 10277–10281.

Qu, A., and Leahy, D.J. (1996). The role of the divalent cation in the structure of the I domain from the CD11a/CD18 integrin. Structure *4*, 931–942.

Rich, R.L., Deivanayagam, C.C., Owens, R.T., Carson, M., Hook, A., Moore, D., Yang, V.W., Narayana, S.V., and Hook, M. (1999). Trench-shaped binding sites promote multiple classes of interactions between collagen and the adherence receptors, $\alpha1\beta1$ integrin and *Staphylococcus aureus* Cna MSCRAMM. J. Biol. Chem. *274*, 24906–24913.

Shimaoka, M., Lu, C., Palframan, R., von Andrian, U.H., Takagi, J., and Springer, T.A. (2001). Reversibly locking a protein fold in an active conformation with a disulfide bond: integrin αL I domains with high affinity and antagonist activity in vivo. Proc. Natl. Acad. Sci. USA *98*, 6009–6014.

Shimaoka, M., Takagi, J., and Springer, T.A. (2002). Conformational regulation of integrin structure and function. Annu. Rev. Biophys. Biomol. Struct. *31*, 485–516.

Shimaoka, M., Xiao, T., Liu, J.-H., Yang, Y., Dong, Y., Jun, C.-D., McCormack, A., Zhang, R., Joachimiak, A., Takagi, J., et al. (2003). Structures of the αL I domain and its complex with ICAM-1 reveal a shape-shifting pathway for integrin regulation. Cell *112*, 99–111.

Springer, T.A. (1994). Traffic signals for lymphocyte recirculation and leukocyte emigration: the multi-step paradigm. Cell *76*, 301–314.

Takagi, J., Petre, B.M., Walz, T., and Springer, T.A. (2002). Global conformational rearrangements in integrin extracellular domains in outside-in and inside-out signaling. Cell *110*, 599–611.

Takagi, J., Strokovich, K., Springer, T.A., and Walz, T. (2003). Structure of integrin $\alpha5\beta1$ in complex with fibronectin. EMBO J. *22*, 4607–4615.

Xiao, T., Takagi, J., Wang, J.-h., Coller, B.S., and Springer, T.A. (2004). Structural basis for allostery in integrins and binding of ligand-mimetic therapeutics to the platelet receptor for fibrinogen. Nature, *432*, 59–67.

Xiong, J.-P., Stehle, T., Diefenbach, B., Zhang, R., Dunker, R., Scott, D.L., Joachimiak, A., Goodman, S.L., and Arnaout, M.A. (2001). Crystal structure of the extracellular segment of integrin $\alpha V\beta3$. Science *294*, 339–345.

Yang, W., Shimaoka, M., Salas, A., Takagi, J., and Springer, T.A. (2004). Inter-subunit signal transmission in integrins by a receptor-like interaction with a pull spring. Proc. Natl. Acad. Sci. USA *101*, 2906–2911.